PROCEEDINGS OF SCIENCE

Drone-based calibration of AugerPrime radio antennas at the Pierre Auger Observatory

Alex Reuzki[a,*] **for the Pierre Auger Collaboration**[b,†]

[a] *RWTH Aachen University, III. Physikalisches Institut A, Otto-Blumenthal-Str., 52074 Aachen, Germany*

[b] *Observatorio Pierre Auger, Av. San Martín Norte 304, 5613 Malargüe, Argentina*

E-mail: spokespersons@auger.org

Radio emissions of extensive air showers can be observed at the Pierre Auger Observatory with the AugerPrime Radio Detector (RD). As part of the AugerPrime upgrade, RD is being installed on 1660 water-Cherenkov detectors on an area of about 3000 km^2 and consists of dual-polarized Short Aperiodic Loaded Loop Antennas (SALLA). To achieve high measurement precision, RD needs to be well-calibrated, which requires the antenna response pattern to be well-known. We introduce a method to measure the directional response of the SALLA using a well-defined biconical antenna mounted to a drone. The drone-based setup possesses active stabilization and precise pointing with the use of a gimbal. Additionally, the drone's position is tracked using differential GPS with O(cm) precision. This setup allows us to precisely extract the antenna response pattern from any direction in the frequency range of 30 – 80 MHz. In a recent in-situ campaign, calibration measurements of the AugerPrime radio detector have been performed. First results of these measurements are presented and compared to simulations.

10th International Workshop on Acoustic and Radio EeV Neutrino Detection Activities (ARENA2024)
11-14 June 2024
The Kavli Institute for Cosmological Physics, Chicago, IL, USA

*Speaker

†Full author list at https://www.auger.org/archive/authors_2024_08.html

PoS(ARENA2024)029

1. Introduction

Extensive Air Showers (EAS) propagating through the Earth's atmosphere emit radio waves [1, 2]. Starting in 2011, the Auger Engineering Radio Array (AERA) is taking data by observing the radio emissions of such air showers and has confirmed the capability of radio measurements in air shower physics [3–5]. The currently ongoing AugerPrime radio upgrade is building on the achievements of AERA, by adding a radio detector (RD) to each water Cherenkov detector (WCD) at the Pierre Auger Observatory [6]. RD will allow probing highly inclined events at the highest energies, well above the AERA capabilities. In Fig. 1 a model of an upgraded WCD is shown, which newly adds a scintillation and the radio detector.

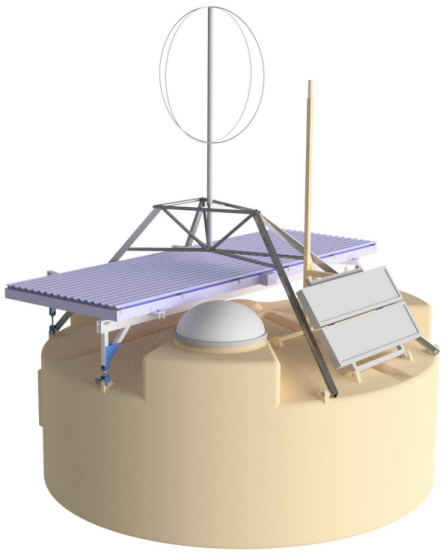

Figure 1: Conceptional illustration of an upgraded SD station. Additionally to the WCD a scintillator (SSD) and radio antenna (RD) is mounted on top. Figure from [7].

RD consists of a dual-polarized short aperiodic loaded loop antenna (SALLA) with one antenna arm aligned for optimal sensitivity in the North-South (NS) direction and the other perpendicular in the East-West (EW) direction. It records signals in the 30 MHz - 80 MHz frequency band with a sampling rate of 250 MHz. As of 03.08.2024, 974 of the total 1660 stations have been upgraded and are taking data. Achieving a high measurement precision of RD requires the antenna response pattern to be well known, which demands careful calibrations. Here, particular challenges are the low-frequency range, equating to a far-field condition of at least 20 m, and the large WCD, which makes measurements in calibration chambers difficult.

In this contribution, we present an in-situ drone-based calibration method, based on previous calibrations for AERA [8]. The method is based on transmission measurements to extract the relative antenna response from a given arrival direction and frequency. A drone is used to position the transmission source in the far field and to point it into a desired arrival direction.

In Sec. 2 the calibration strategy is explained in detail. Sec. 3 focuses on the calibration setup with special emphasis on the usage of a differential GPS (dGPS) module. In Sec. 4 calibration

measurements are presented, along with the most important corrections and uncertainties. The results of an example flight are shown.

2. Calibration Strategy

As the general strategy, the calibration of RD is divided in two complementary tasks, the absolute and the relative calibration. The absolute calibration uses the galactic radio background as a reference signal and extracts the antenna response's absolute scale as a function of frequency [9, 10]. The relative calibration extracts the direction-dependent antenna response pattern for each frequency via transmission measurements. The combination of absolute and relative calibrations provides a full calibration of the RD. This work describes the relative calibration.
The antenna response pattern is characterized by the Vector Effective Length (VEL) $\vec{H}$. The VEL relates the response voltage U at the antenna output to the incoming electric field $\vec{E}$. In Fourier space, it is defined as

$$\mathcal{U}(\Phi, \Theta, f) = \vec{H}(\Phi, \Theta, f) \cdot \vec{\mathcal{E}}(f). \tag{1}$$

In spherical coordinates, $\vec{H}$ is a superposition of a horizontal component H_ϕ and a meridional component H_θ. The absolute values of these components can be determined in transmission measurements for the polarizations $k = \phi, \theta$ using

$$|H_k(\phi, \theta, f)| = \sqrt{\frac{4\pi Z_\mathrm{R}}{Z_0}} R \sqrt{\frac{P_{\mathrm{r},k}(\phi, \theta, f)}{P_t(f) G_{\mathrm{abs,t}}(f)}}. \tag{2}$$

Required is a well-known transmission source with the transmitted power $P_t(f)$ of frequency f and absolute Gain $G_{\mathrm{abs,t}}$. $P_{\mathrm{r},k}$ is the received power at the antenna. The azimuth angle ϕ and zenith angle θ and the distance to the antenna R describe the location of the transmission source in spherical coordinates. Z_R is the read-out impedance, Z_0 is the impedance of free space. Eq. 2 only holds for a transmission source in the far field, where the electric and magnetic fields fall off with $1/R$. A more detailed derivation can be found in [8]. Note that only the received power depends on the position of the source since every other quantity is only frequency dependent. As a result, only the received power and location of the source need to be known to extract the direction-dependent sensitivity of the antenna. To achieve a far field distance for any arrival direction, a drone is used to place the transmission source in the desired location. In this way, one can cover all possible arrival directions and therefore probe the full antenna pattern. The drone is autonomously piloted using pre-programmed flight paths in the software Litchi [11]. The flight paths are defined by waypoints at which the drone stops to stabilize, enabling an antenna measurement to be recorded. Additionally, the autonomous flight allows to automatically aim the transmission source at the antenna by defining a point of interest (POI). During the flight, the drone directs the transmission antenna toward the POI, which is predefined by the RD's center. The pre-programmed flight path of the example flight is shown in Fig. 2 (left). A full coverage of the antenna pattern results in a dome-shaped flight path with the RD at its center.

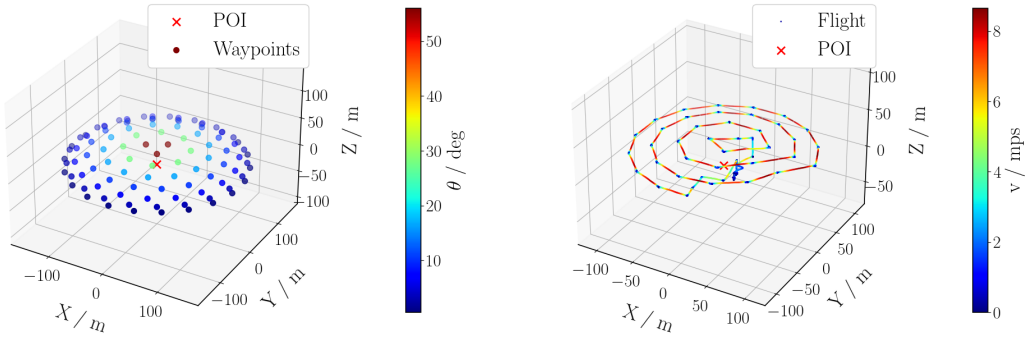

Figure 2: *Left:* Pre-programmed flight path in the form of waypoints and a Point of Interest (POI). The drone flies to each waypoint and stops. *Right:* Recorded GPS data for the example flight. The color indicates the velocity of the drone. The individual waypoints at which the drone stopped are visible, indicated through dark blue dots.

3. Calibration Setup

The core of the measurement setup is a drone of the type DJI M600 Pro [12] which is shown in Fig. 3. The drone is powered by six lithium polymer batteries and achieves a flight duration with no payload of > 30 min and ≈ 15 min with the maximum payload. The landing gear of the drone is retractable and is therefore not obstructing the transmission antenna's movement nor does it harm its radiation pattern. Furthermore, the drone has a built-in GPS with a vertical accuracy of 1.5 m and a horizontal accuracy of 0.8 m. This GPS is used for navigation and as a backup system to the high-accuracy differential GPS, which will be detailed below. In addition to the direction-dependence of the SALLA's antenna pattern, the antenna pattern of the transmission antenna also has a direction-dependence. Consequently, it is important to align the transmission antenna toward the antenna on the ground. This task is accomplished by introducing a motorized gimbal under the drone of the type Ronin MX, developed by DJI. The gimbal adjusts the transmission antenna's alignment and stabilizes it simultaneously. It is controlled by three independently motorized axes, controlling the pitch, roll, and yaw. A yaw represents a rotation about the z-axis (up/down), the pitch about the y-axis (left/right), and the roll about the x-axis (forward) of an object. The yaw and roll are controlled to ensure stabilization, while the pitch is controlled to ensure stabilization as well as proper alignment. The gimbal is not only used to stabilize and align but also to house the electronics of the signal chain, which consists of three main components, a signal generator, an amplifier, and an antenna. First, the signal is generated with the reference spectrum generator RSG 1000, by TESEQ [13]. The reference spectrum generator (RSG) produces a comb spectrum between 1 MHz and 1 GHz in 5 MHz steps.

Figure 3: The DJI Matrice M600 Pro together with the calibration equipment mid-flight (left) and stationary (right).

With such a signal spectrum, we can probe eleven frequencies between 30 – 80 MHz simultaneously. Secondly, the signal is amplified by 24.7 dB using a ZFL-2500VH+ [14] amplifier to ensure a high signal above noise for far-field distances. Lastly, the amplified signal is supplied to an antenna. The antenna in use is the biconical open cone antenna BBOC 9217 [15] with a broad bandwidth between 30 MHz and 1 GHz. The transmission antenna can be rotated by 90° before a flight to change the polarization of the transmitted signal to a horizontal/ϕ-polarized or meridional/θ-polarized signal and thereby change the probed VEL. To reduce systematic uncertainties caused by the accuracy of the built-in GPS, an additional differential GPS (dGPS) module is introduced. In contrast to the comparatively low accuracy of the built-in GPS of $\mathcal{O}$(m), the dGPS can achieve an accuracy of up to 1 cm. The dGPS setup consists of a dGPS chip on top of the drone and a base station on the ground. The high accuracy of the dGPS refers to the relative position between the drone and the base station.

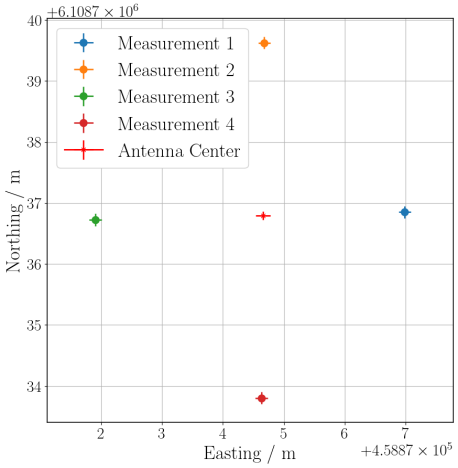

Figure 4: The results of the cross-measurement used for the example flight. The antenna center is determined with an accuracy of 17 cm.

To achieve an appropriate position accuracy the relative position between the base station and the RD has to be known. This is accomplished by performing a *cross-measurement* before or after a calibration measurement. The drone is manually placed in a cross shape around the SALLA while being aligned with the North-South and East-West directions. The position of RD, in particular the antenna center of the SALLA, is determined by drawing lines between two opposite measurements. The relative position between the drone and the RD can be obtained by combining the relative position measurement of the drone with the relative measurement of the RD. In Fig. 4 the cross-measurement conducted for the example flight is shown. An accuracy of 17 cm has been achieved for the relative position of RD. This is a combination of the error of placing the drone in the correct position, the unevenness of ground around the RD, and error propagation to the antenna center.

4. Measurement of the SALLA Direction-Dependent Sensitivity

Using the previously described strategy and its setup, an in-situ calibration campaign has been conducted in November 2023. The campaign lasted a total of three weeks and included 64 flights. With an average flight duration of approx. 13 min a total flight duration of $\approx$ 13 h 21 min has been achieved. Here we present first results of one example flight performed using a ϕ-polarized transmission signal. We show relevant corrections and uncertainties of the example flight. The flight path recorded with the built-in GPS of the example flight is shown in Fig. 2 (right). The color of each position represents the total velocity of the drone. The waypoints, at which the drone came to a full stop, are visible as dark blue dots.

Corrections

To ensure a correct extraction of the VEL, the measurements are subjected to various corrections. The current largest correction is the correction for misalignment between the transmission antenna and RD. The biconical antenna radiation pattern is in good approximation that of a regular dipole antenna with a dependency $|E| \propto \sin\alpha$ relative to the dipole axis and $|E| \propto$ const perpendicular to the dipole axis. The angle α is calculated by first performing an extrinsic rotation corresponding to the gimbal orientation and afterward, an intrinsic rotation corresponding to the drone angles. The total rotation is expressed as the product of rotation matrices $R_{\text{tot}} = R^D_{\text{roll}} \cdot R^D_{\text{pitch}} \cdot R^D_{\text{yaw}} \cdot R^G_{\text{yaw}} \cdot R^G_{\text{pitch}} \cdot R^G_{\text{roll}}$, where D refers to the drone and G to the gimbal. The misalignment amounts to corrections ranging from $< 0.1\%$ up to 3%. Further corrections, like the influence of the drone on the transmission antenna's radiation pattern, are being investigated.

Uncertainties

The total position uncertainty is a combination of the above-mentioned uncertainty on the RD's position and the uncertainty on the drone's position. A position accuracy of on average 25 cm has been achieved. In addition to the uncertainty on the RD's position, a time uncertainty of the drone's dGPS data dominates this uncertainty. This leads to a systematic uncertainty on the VEL of 0.2%. Additional systematic uncertainties are being investigated, including the uncertainty on the correction of drone influence and temperature shifts of certain electronic components in received and transmitted signals. They are expected to not have a large impact on the total systematic uncertainty. The statistical uncertainty is dominated by subtracting the background noise. Before

or after a flight background data have been recorded. An average background spectrum with corresponding noise is calculated and subtracted. The background noise is assigned as a statistical uncertainty to the calibration data. This leads to an average statistical uncertainty of 0.6%.

First Results

The first results for the example flight with ϕ-polarized signal at 55 MHz are shown in Fig. 5. The flight contained a total of 58 measurements. As seen in Fig. 2 (right), the flight consisted of four rings at four different zenith angles. In Fig. 5, measurements of the three flight rings with more than three waypoints are presented. The red line shows the simulated antenna pattern for RD. The simulation has been produced with the 4NEC2 software [16] and has also been used in previous studies [17, 18]. Since the performed calibration is relative, the simulation pattern is normalized to the recorded measurements. The normalization has been performed for each zenith ring individually. The uncertainties are small and therefore barely visible. The general shapes of data and simulation are in overall agreement. The average deviation from the normalized simulation amounts to 7%, which motivates further investigation on potential additional corrections and uncertainties.

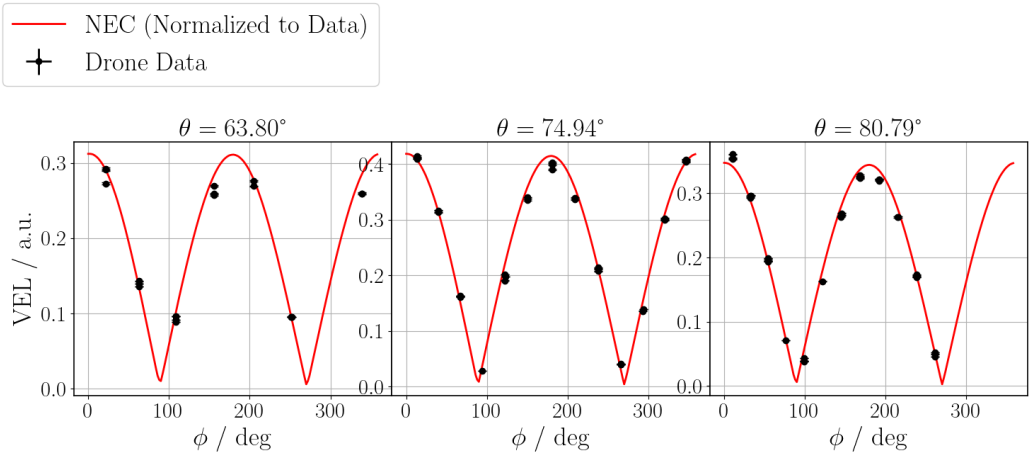

Figure 5: First results of the example flight calibration measurements for the East-West channel at 55 MHz are shown. The results are split into three rings of different zenith angles. Statistical uncertainties are shown as error bars and systematic uncertainties as error caps. The simulated pattern is shown as a red line and normalized to the recorded data for each slice.

5. Summary and Outlook

A drone-based transmission setup has been developed utilizing a differential GPS to achieve high position accuracy. The setup also includes a gimbal which introduces automatic pointing and stabilization. In a calibration campaign lasting three weeks, the setup was used to perform RD measurements by determining the vector effective length of the antenna, which describes the antenna response to an incoming electric field. First results have been presented, which are in

overall agreement with simulations.

As seen in Fig. 5, the data is sparsely distributed from which a need for interpolation arises. Information field theory (IFT) is a strong tool, that allows us to interpolate high-dimensional fields using Bayesian statistics. We plan to use IFT to interpolate the calibration data in three dimensions (f, θ, ϕ) and simultaneously produce Bayesian uncertainties [19]. Combining the interpolation and an analysis of the whole data set will provide valuable insight into the direction-dependent antenna pattern.

References

[1] J. Jelley *et al.*, *Nature* **205** (1965) 327-328.

[2] R. Porter *et al.*, *Nature* **213** (1967) 1107.

[3] A. Abdul Halim *et al.*, *Phys. Rev. D.* **109** (2024) 022002.

[4] T. Huege *et al.*, *EPJ Web Conf.* **210** (2019) 05011.

[5] C. Glaser, Ph.D. thesis, RWTH Aachen University, 2017.

[6] The Pierre Auger Collaboration, *Nucl. Instrum. Meth.* **A 798** (2015) 172 - 213.

[7] J. Hörandel *et al.*, *EPJ Web Conf.* **210** (2019) 06005.

[8] R. Krause, Ph.D. thesis, RWTH Aachen University, 2018.

[9] T. Fodran *et al.*, *PoS* **ICRC2021** (2021) 270.

[10] R. de Almeida *et al.*, *PoS* **ICRC2023** (2023) 279.

[11] https://flylitchi.com/.

[12] https://www.dji.com/de/matrice600-pro/info.

[13] https://accelonix.nl/wp-content/uploads/Teseq_RSG_1000.pdf.

[14] https://www.minicircuits.com/WebStore/dashboard.html?model=ZFL-2500VH%2B.

[15] https://schwarzbeck.de/Datenblatt/91149217.pdf.

[16] https://www.qsl.net/4nec2/.

[17] U. Giaccari *et al.*, *PoS* **ARENA2022** (2022) 042.

[18] T. Fodran *et al.*, *PoS* **ARENA2022** (2022) 043.

[19] A. Reuzki, master's thesis, RWTH Aachen University, 2023.